Aquaporins Have Regional Functions in Development of Refractive Index in the Zebrafish Eye Lens

Kehao Wang,[1] Irene Vorontsova,[2,3] Masato Hoshino,[4] Kentaro Uesugi,[4] Naoto Yagi,[4] James Ewbank Hall,[2] Thomas Friedrich Schilling,[3] and Barbara Krystyna Pierscionek[5,6]

[1]Beijing Advanced Innovation Centre for Biomedical Engineering, Key Laboratory for Biomechanics and Mechanobiology of Ministry of Education, School of Biological Science and Medical Engineering, Beihang University, Beijing, China
[2]Department of Physiology and Biophysics, University of California Irvine, Irvine, California, United States
[3]Department of Developmental and Cell Biology, University of California Irvine, Irvine, California, United States
[4]Japan Synchrotron Radiation Research Institute, Hyogo, Japan
[5]School of Life Sciences and Education, Staffordshire University, Stoke-on-Trent, United Kingdom
[6]Faculty of Health, Education, Medicine and Social Care, Chelmsford Campus, Anglia Ruskin University, United Kingdom

Correspondence: Barbara Krystyna Pierscionek, Faculty of Health, Education, Medicine and Social Care, Chelmsford Campus, Anglia Ruskin University, Bishop Hall Lane, Chelmsford, Essex CM1 1SQ, UK; barbara.pierscionek@aru.ac.uk.

Received: December 7, 2020
Accepted: February 17, 2021
Published: March 16, 2021

Citation: Wang K, Vorontsova I, Hoshino M, et al. Aquaporins have regional functions in development of refractive index in the zebrafish eye lens. *Invest Ophthalmol Vis Sci.* 2021;62(3):23. https://doi.org/10.1167/iovs.62.3.23

Purpose. In the eye lens, cytosolic protein concentrations increase progressively from the periphery to the center, contributing to the gradient of refractive index (GRIN). Aquaporins are membrane proteins of lens fiber cells that regulate water transport and adhesion and interact with cytoskeletal proteins. This study investigates how these membrane proteins contribute to proper development of the lens GRIN.

Methods. Loss-of-function deletions of *aqp0a* and/or *aqp0b* in zebrafish were generated using CRISPR/Cas9 gene editing. Lenses of single *aqp0a*$^{-/-}$ mutants, single *aqp0b*$^{-/-}$ mutants, and double *aqp0a*$^{-/-}$/*aqp0b*$^{-/-}$ mutants from larval to elderly adult stages were measured using x-ray Talbot interferometry at SPring8 in Japan. The three-dimensional GRIN profiles in two orthogonal cross-sectional planes of each lens were analyzed and compared with in vivo images and previous results obtained from wild-type lenses.

Results. Single *aqp0a*$^{-/-}$ mutants tended to show asymmetric GRIN profiles, with the central plateau regions shifted anteriorly. Single *aqp0b*$^{-/-}$ mutants had smooth, symmetric GRIN profiles throughout development until spoke opacities appeared in several extremely old samples. Double *aqp0a*$^{-/-}$/*aqp0b*$^{-/-}$ mutants showed lower magnitude GRIN profiles, as well as dips in the central plateau region.

Conclusions. These findings suggest that Aqp0a and Aqp0b have region-specific functions in the lens: Aqp0a is active peripherally, regulating centralization of the plateau region, and this function cannot be compensated for by Aqp0b. In the lens center, either Aqp0a or Aqp0b is required for formation of the plateau region, as well as for the GRIN to reach its maximum magnitude in mature lenses.

Keywords: zebrafish, eye development, refractive index, eye lens, aquaporins

Cataract, an opacification of the lens of the eye, remains a leading cause of blindness in the world and is most commonly a manifestation of aging or a secondary consequence of systemic disease. This sight-impairing condition has been associated with various mutations and consequent modifications in the organization of lens proteins. The most common of these are the cytosolic crystallins and the proteins that are responsible for maintaining lens structure and physiology: the connexins and Aquaporin 0 (AQP0), also known as membrane intrinsic protein. Without an ordered arrangement of crystallins and water, the lens loses transparency. The vertebrate lens consists of fiber cells arranged in concentric layers that are covered by a single layer of epithelial cells at the anterior surface.[1] Crystallins in the cytoplasm of lens fiber cells vary in concentration across the lens (reviewed in Reference 2); connexins and aquaporins in lens fiber cell membranes regulate the transmission of water and small molecules between adjacent fiber cells and extracellular space. The lens transmits light to the retina, and the refractive power of any lens is determined by its surface curvatures and its density, or refractive index. The varying distributions of the crystallin proteins in the eye lens create a gradient of refractive index (GRIN), which is essential for high image quality (reviewed in Reference 2).

We previously[3] demonstrated a coincidence between periods of rapid growth of the zebrafish lens GRIN profile and dramatically increased expression of three crystallin classes, α-, βB3-, and γS-crystallin.[4] Spatial variations across the lens in the membrane refractive index have also been reported,[5] but how different membrane proteins contribute to development of the GRIN profile remains largely unknown.

Aquaporins allow passage of water across biological cell membranes.[6] Mammalian lens epithelial cells express AQP1 and AQP5, and the lens fiber cells express AQP0 and AQP5.[7] AQP0 is the most abundant membrane protein in lens fiber

cells.[8,9] Apart from transporting water, AQP0 is also thought to behave as a cell-to-cell adhesion molecule for maintaining order and transparency of the lens,[9–11] and it interacts with lens cytoskeletal proteins[12,13] and gap junctions.[14,15] Studies in mice suggest that AQP0 regulates both the mechanical and optical functions of the lens, as stiffness of the lens correlates directly with amounts of AQP0 protein.[16] Lenses expressing only 50% of AQP0 protein have significantly lower optical refracting power than wild-type (WT) lenses,[17] and these mutant lenses scatter light and exhibit spherical aberration.[18] These defects likely reflect roles for AQP0 in the development of the lens GRIN.

Mammalian AQP0 is mainly located at the interlocking protrusions found at the corners of fiber cell membranes that regulate the structural order and stability of the lens.[9] With greater depth within the lens, the AQP0 C-terminus undergoes proteolytic cleavage leading to the thinner junctions predominant in the lens center.[6,19] These thin junctions are likely to convert the AQP0 proteins into pure adhesion molecules,[6] although C-terminal truncations do not impair AQP0 permeability.[20] AQP0 is also essential for the maintenance of interlocking protrusions of fiber cells. In mature fiber cells of Aqp0$^{-/-}$ knockout mice, these protrusions are elongated, deformed, and fragmented, resulting in loss of integrity and nuclear cataract.[9] The functions of AQP0 thus change from the lens surface to the lens core as it undergoes cleavage and other posttranslational modifications, and the adhesive function may have greater importance in the lens center (reviewed in Reference 21).

As a result of a whole genome duplication event in the teleost lineage, zebrafish have two orthologs of *AQP0*: *aqp0a* and *aqp0b*.[22,23] Some functions of the mammalian AQP0 are also found in these zebrafish counterparts and have been at least partially separated.[24–26] This sub-functionalization of Aqp0a and Aqp0b allows us to discern some of the functions of the single mammalian ortholog. Knockdown or functional knockout of either gene in zebrafish causes temporary embryonic cataract,[25,26] but transparency returns around 4 days post-fertilization (dpf), indicating possible compensation by other mechanisms. Aqp0a has a unique role in stabilizing the anterior lens suture in older lenses, as well as centralization of the lens nucleus, an essential process in the development of zebrafish lens optics.[26] Thus, the water transport feature of Aqp0a likely facilitates these processes,[24,26] but it remains unclear if Aqp0a or Aqp0b plays a role in the development of refractive properties of the lens.

Using the same measuring technology (x-ray Talbot interferometry) employed in our previous study of GRIN profile development in WT lenses,[3] the aim of the present study was to test if Aqp0a or Aqp0b is required for the development of the lens GRIN profile by using loss-of-function zebrafish mutants.[26]

Methods

Sample Preparation

The animal protocols used in this study adhere to the ARVO Statement for the Use of Animals in Ophthalmic and Vision Research and were approved by the Institutional Animal Care and Use Committee of the University of California, Irvine. Zebrafish (AB strain) were raised and maintained under standard laboratory conditions.[27] CRISPR/Cas9-mediated gene editing was used to create deletions in *Danio rerio aquaporin 0a* (*aqp0a*), also known as major intrinsic protein of lens fiber a (*mipa*) (Gene ID 445140), or *Danio rerio aquaporin 0b* (*aqp0b*), also known as major intrinsic protein of lens fiber b (*mipb*) (Gene ID 553420), as described previously.[26] CRISPR/Cas9-injected F0 fish were outcrossed, F1s were selected for out-of-frame deletions in *aqp0a* or *aqp0b*, and stable mutant lines were raised for further analysis. Homozygotes for mutations in both genes were raised and intercrossed to generate double homozygous *aqp0a*$^{-/-}$/*aqp0b*$^{-/-}$ mutants. Maternal-zygotic (MZ) null mutant offspring of these double mutants were assessed and compared with WT AB strain zebrafish.

Zebrafish were anesthetized in tricaine (MS-222; Sigma-Aldrich, St. Louis, MO, USA). For in vivo eye transparency assessment, a fiberoptic light source (KL1500; Schott AG, Mainz, Germany) was used for oblique illumination from two sides to visualize opacities. Fish standard length was measured following previously established guidelines.[28] Lenses were dissected from animals in BioWhittaker Dulbecco's modified Eagle's medium (DMEM) with 25-mM HEPES and 4.5 g/L glucose without L-glutamine (Lonza, Inc., Morristown, NJ, USA) at room temperature. For assessment of transparency, dissected lenses were visualized under both darkfield (DF) and brightfield (BF) illumination with an Olympus SZX12 microscope using an Olympus DP70

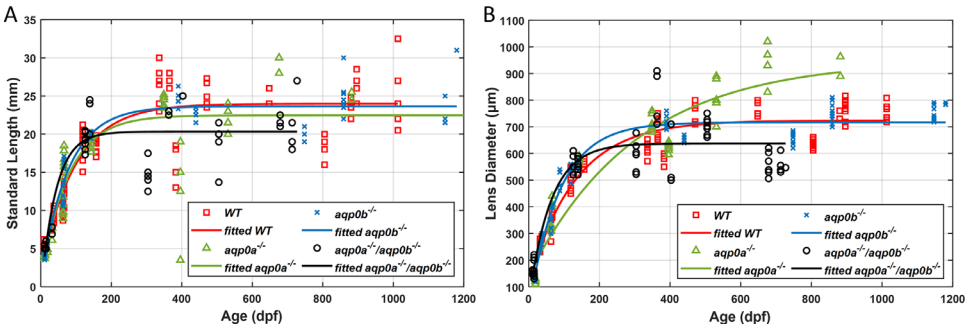

Figure 1. Zebrafish *aqp0* mutant lens growth. Zebrafish standard length (**A**) and lens diameter (**B**) as a function of age (dpf) for WT, *aqp0a*$^{-/-}$, *aqp0b*$^{-/-}$, and double *aqp0a*$^{-/-}$/*aqp0b*$^{-/-}$ mutants. WT and *aqp0b*$^{-/-}$ standard length growth plateaued at ~24 mm after ~350 dpf (**A**, *red* and *blue*); in *aqp0a*$^{-/-}$, at ~23 mm after ~350 dpf (**A**, *green*). The double mutant standard length plateaued at ~20 mm after the age of ~180 dpf (**A**, *black*). Lens growth in WT and *aqp0b*$^{-/-}$ plateaued at ~710 µm (**B**, *red* and *blue*), which corresponds to ~500 dpf; there was no plateau for samples from *aqp0a*$^{-/-}$ mutants with a maximum attained value of 900 µm at 900 dpf (**B**, *green*), and lens growth plateaued at ~640 µm in double homozygotes after ~230 dpf (**B**, *black*).

Investigative Ophthalmology & Visual Science

Table 1. Coefficients of Growth Curves Fitted to Exponential Growth Model ($y = a + be^{cx}$, r^2) for WT, *aqp0a*$^{-/-}$, *aqp0b*$^{-/-}$, and Double *aqp0a*$^{-/-}$/*aqp0b*$^{-/-}$ Mutants

	Figure 1A, Standard Fish Length Versus Age				Figure 1B, Lens Diameter Versus Age			
	WT	*aqp0a*$^{-/-}$	*aqp0b*$^{-/-}$	*aqp0a*$^{-/-}$/*aqp0b*$^{-/-}$	WT	*aqp0a*$^{-/-}$	*aqp0b*$^{-/-}$	*aqp0a*$^{-/-}$/*aqp0b*$^{-/-}$
a	23.98	22.47	23.65	20.33	724	950	717	637
b	−21.83	−21.37	−22.63	−21.22	−615	−807	−699	−591
c	−0.010	−0.013	−0.013	−0.023	−0.008	−0.003	−0.011	−0.016
r^2	0.87	0.75	0.93	0.74	0.94	0.90	0.96	0.82

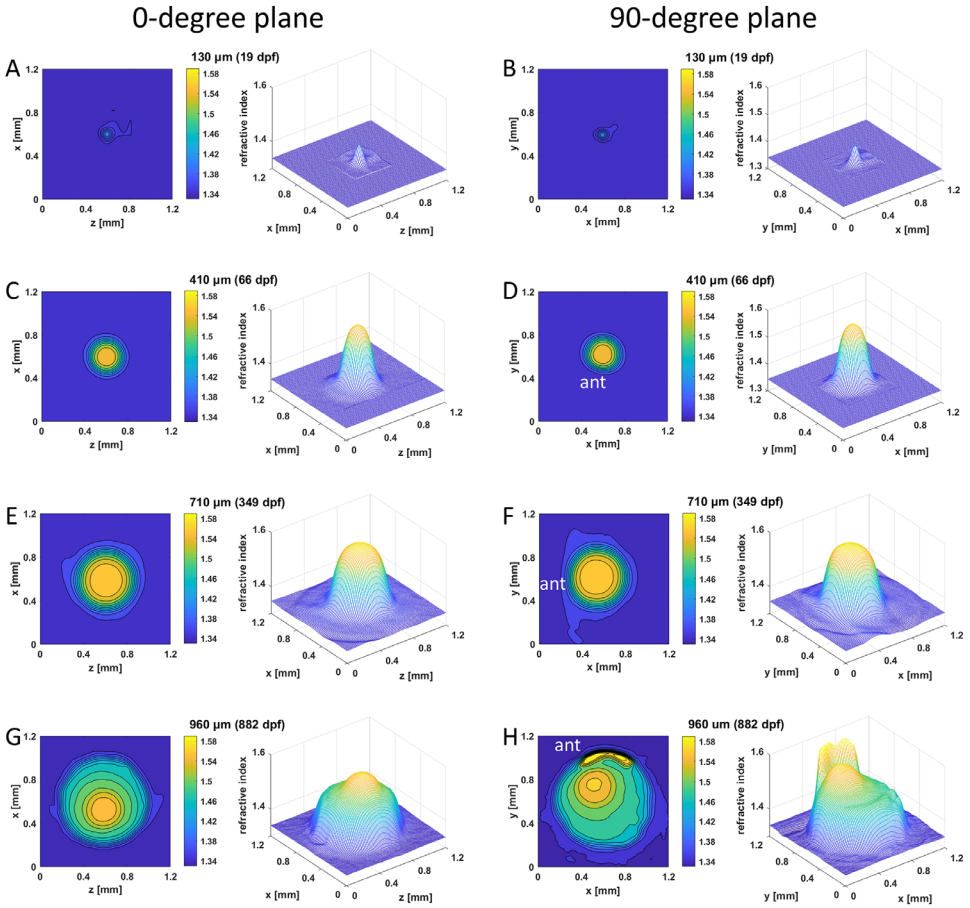

Figure 2. GRIN distributions in *aqp0a*$^{-/-}$ lenses. Two-dimensional contour plot (*left panels*) and 3D mesh plot (*right panels*) of GRIN distributions in *aqp0a*$^{-/-}$ lenses in the 0°plane, representing the equatorial plane (*left column*), and 90° plane, representing the axial plane (*right column*), of four selected lenses with diameters ranging from 130 to 960 µm at specified dpf. The magnitude of refractive index is color coded according to the color bar displayed on the right side of each contour plot. Anterior (ant) is the surface of the lens where light enters the lens. See Supplementary Figure S2 for higher magnifications of **A** and **B**.

digital camera with an Olympus DP Controller (2.1.1.183; Olympus Corporation, Tokyo, Japan). Lenses were transported to the measurement facility at room temperature in Eppendorf tubes in DMEM supplemented with 1 µg/mL of penicillin/streptomycin and were measured at the SPring-8 synchrotron radiation facility within 1 week of dissection. Samples where DMEM had turned yellow were discarded, as this indicated degradation of the sample. Data collected once per year over 4 consecutive years (2016–2019) were merged for this study. A total of 42 *aqp0a*$^{-/-}$ lenses ages 19 to 882 dpf, 92 *aqp0b*$^{-/-}$ lenses ages 19 to 1147 dpf, and 54 *aqp0a*$^{-/-}$/*aqp0b*$^{-/-}$ lenses ages 15 to 713 dpf were measured. An additional group of 24 old WT lenses ages 1013, 1541, and 1939 dpf were included for comparison. Numbers and ages of samples for each genotype are listed in Supplementary Table S1.

Synchrotron-Based X-Ray Phase Tomography

Refractive index distribution in each lens was measured using x-ray phase tomography based on X-ray Talbot interferometry located at the bending magnet beamline BL20B2 at the SPring-8.[29,30] A monochromatic X-ray beam was fine-tuned to 25 keV and passed through a nickel phase grating (G1) with a pattern thickness of 4.35 µm and a gold absorption grating (G2) with a pattern thickness of

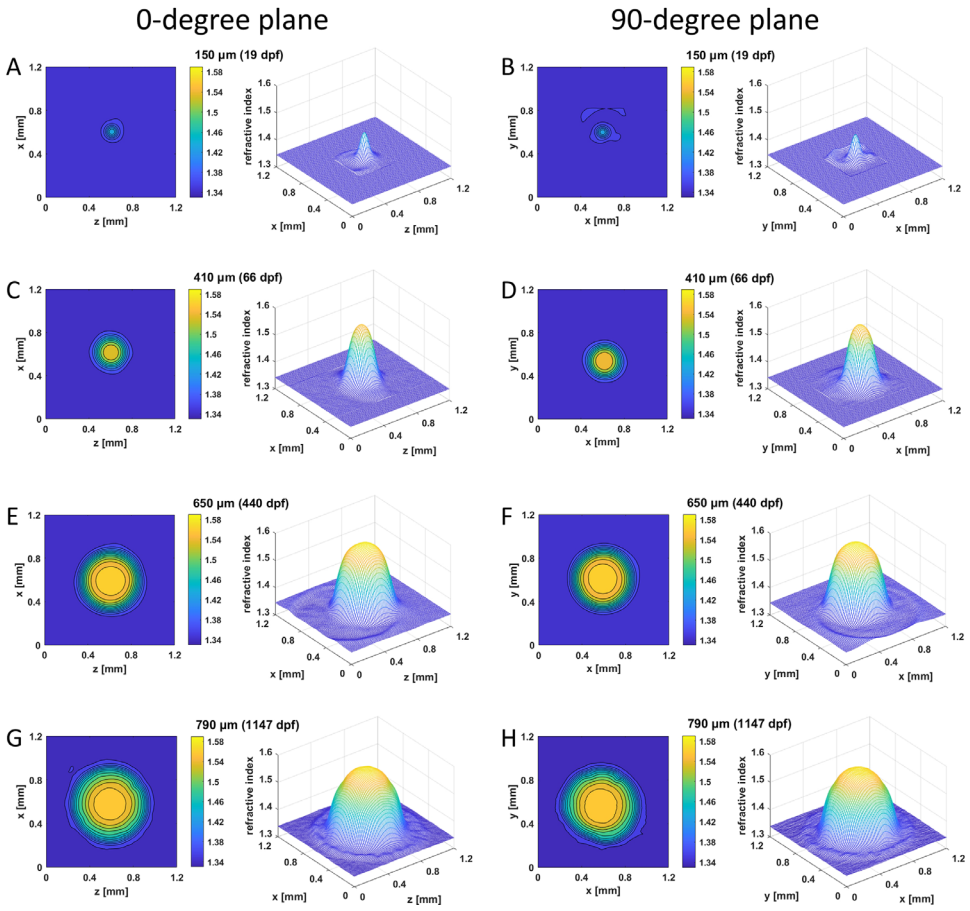

Figure 3. GRIN distributions in *aqp0b*$^{-/-}$ lenses. Two-dimensional contour plot (*left panels*) and 3D mesh plot (*right panels*) of GRIN distributions in the 0° plane, representing the equatorial plane (*left column*), and 90° plane, representing the axial plane (*right column*), of four selected lenses with diameters ranging from 130 to 790 µm at specified dpf. See Supplementary Figure S2 for higher magnifications of **A** and **B**.

110 µm in sequence. Both transmission gratings have a pitch size of 4.8 µm and a pattern size area of 50 × 50 mm^2. Moiré fringe patterns produced by X-ray beams passing through the sample and the two gratings are detected by a complementary metal-oxide semiconductor detector (ORCA-Flash4.0; Hamamatsu Photonics, Hamamatsu, Japan). G2 was shifted relative to G1 with a Piezo stage using a five-step fringe-scan method for phase retrieval. Each sample was immobilized within a 2% agarose gel and fixed on a rotator during measurement, creating 900 projection images. Integration of the differential phase images produced by the scans created the final phase images used for tomographic reconstruction. The obtained phase shift per pixel can be used to determine the X-ray refractive index differences, from which protein concentrations, as well as the refractive indices of the lens, can be calculated.[31,32] Calibration of the interferometry was performed at the beginning of each day of measurement using five different solutions of known density[32,33] and comparing the experimentally measured phase shift per pixel to the theoretical calculated value. Linear relationships were found over the tested range of concentrations, and this linear relationship covered the refractive index range measured in this work. The three-dimensional refractive index values of each lens were processed with MATLAB 2019b (MathWorks, Natick, MA, USA). Two-dimensional (2D) plots with isoindicial index contours and three-dimensional (3D) gradient index profiles in the equatorial and axial planes of each lens were generated (Supplementary Fig. S1 shows the orientations of equatorial and axial planes). When discernible, 2D images of lenses were reconstructed from 3D stacks in two perpendicular planes: 0° and 90° orientations (representing the equatorial and axial planes, respectively; see Figs. 2–4). The position of the lens nucleus was largely used as a guide, as it is closer to the anterior pole in younger WT lenses and in some aged mutants. Lens diameter was measured in equatorial lens sections by fitting a circle to the outermost line in the contour plot using SolidWorks 2018 (SolidWorks, Waltham, MA, USA). MATLAB 2019b was used for statistical analysis.

Results

Development of GRIN in Aqp0 Mutant Zebrafish Lenses

The GRIN profiles in WT, *aqp0a*$^{-/-}$, and *aqp0b*$^{-/-}$ single mutants and double *aqp0a*$^{-/-}$/*aqp0b*$^{-/-}$ mutant zebrafish lenses were measured from larval to elderly adult stages. Zebrafish standard length and lens diameter were used as indicators of lens developmental stages, as in our previous study.[3] To verify if standard length or lens

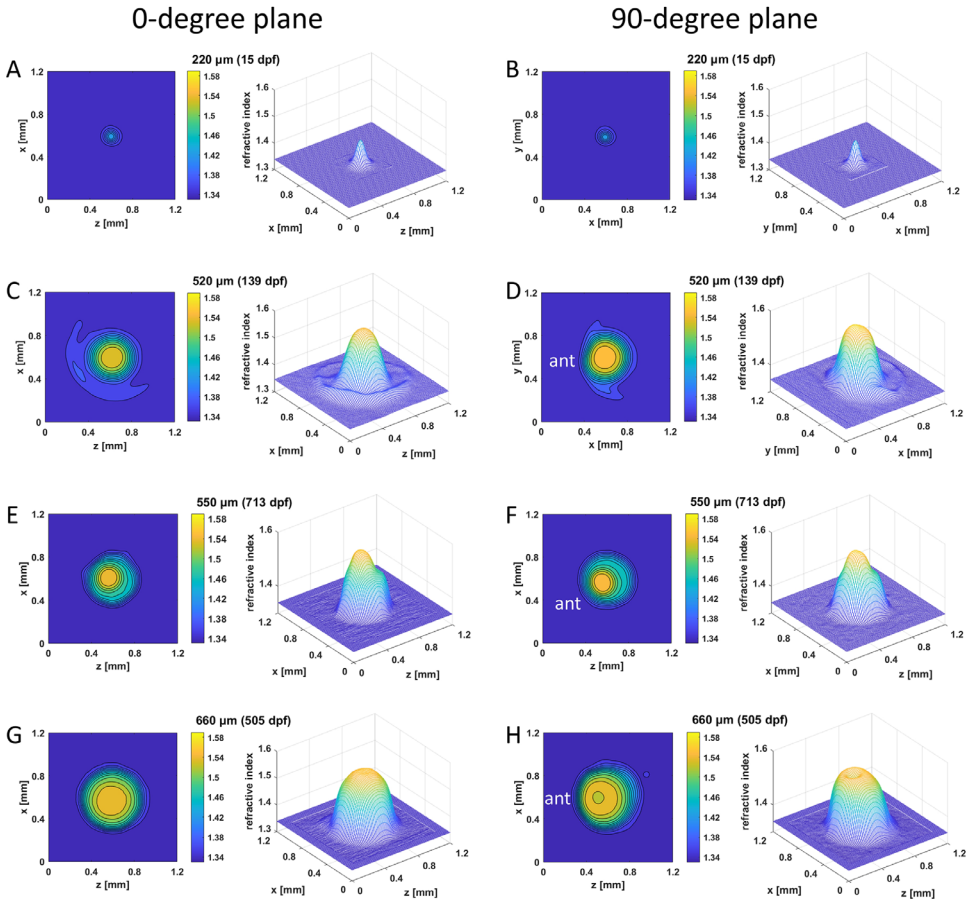

Figure 4. GRIN distributions in double *aqp0a*$^{-/-}$/*aqp0b*$^{-/-}$ mutant lenses. Two-dimensional contour plots (*left panels*) and 3D mesh plots (*right panels*) of GRIN distributions in the 0° plane, representing the equatorial plane (*left column*), and 90° plane, representing the axial plane (*right column*), of four selected lenses with diameters ranging from 220 to 660 µm (15–713 dpf). Equatorial aspect is perpendicular to the optic axis; axial aspect contains the optic axis. Anterior (ant) is the surface of the lens where light enters the lens. See Supplementary Figure S2 for higher magnifications of **A** and **B**.

diameter of the mutants was affected in comparison to WT, the parameters were fitted to an exponential growth model and compared to results from WT lenses over the same age range (Figs. 1A , B; fitting coefficients are listed in Table 1). The *aqp0b*$^{-/-}$mutants revealed growth trends similar to those for WT for both parameters, including an initial rapid growth followed by a gradual decrease in growth rate, plateauing around 400 dpf. *aqp0a*$^{-/-}$ mutants varied in standard length beyond 400 dpf and, although lens diameter continuously grew, it did not reach as high a plateau as in WT siblings. Growth in either parameter of double *aqp0a*$^{-/-}$/*aqp0b*$^{-/-}$ mutants was compromised after 200 dpf. A range of values in both standard length and lens diameter was observed within the same age cohorts for each genotype, indicating growth variability. Variations in lens diameter were smaller than variations in the standard length. Lenses of fish beyond ~800 dpf were so severely opacified and structurally deteriorated that they could not withstand manipulation; hence, double *aqp0a*$^{-/-}$/*aqp0b*$^{-/-}$ mutant analysis was restricted to younger animals.

We measured both 2D refractive index contours and 3D mesh plots of the GRIN profiles in two orthogonal planes for four selected *aqp0a*$^{-/-}$ lenses with diameters of 130 µm (19 dpf), 410 µm (66 dpf), 710 µm (349 dpf), and 960 µm (882 dpf) (Fig. 2). A GRIN profile was evident even at 19 dpf (Figs. 2A, B; Supplementary Figs. S2A, B). With increasing diameter, lens size and GRIN profile magnitude both increased dramatically. Lenses had circular contours of refractive index and smooth, symmetrical GRIN profiles in both the 0° and 90° planes up to 710 µm in diameter (Figs. 2A–F). The oldest lenses exhibited two distinct regions in the mesh plot of GRIN profiles: one in the 0° plane (Fig. 2G) and a local, secondary high peak in the 90° plane (Fig. 2H). The lens nucleus, exhibiting the highest refractive index, was clearly localized asymmetrically in the 90° orientation closer to the anterior pole (Figs. 2F, H).

Refractive index distributions were measured in two orthogonal planes for four selected *aqp0b*$^{-/-}$ lenses with diameters of 150 µm (19 dpf), 410 µm (66 dpf), 650 µm (440 dpf), and 790 µm (1147 dpf) (Fig. 3; Supplementary Figs. S2C, D). Spherical contours and smooth, symmetrical mesh plots were seen across all developmental stages. The plateau region barely increased in size in lenses from 650 to 790 µm in diameter, and the shape of the GRIN profile in the oldest lenses was close to parabolic (Figs. 3G, H). Note that spatial resolution was limited for lenses below 200 µm in diameter; hence, the profile shapes for these lenses were less detailed than for larger lenses.

More irregularities were found in the shape of 2D contours and 3D mesh plots of the double

Investigative Ophthalmology & Visual Science

Table 2. Frequency of Dysfunctional GRIN Profile of WT, Single *aqp0a*$^{-/-}$ Mutants, Single *aqp0*$^{-/-}$ Mutants, and Double *aqp0a*$^{-/-}$/*aqp0b*$^{-/-}$ Mutants in Four Different Age Groups

	Age Group			
Genotype	**0–200 dpf**	**200–500 dpf**	**500–900 dpf**	**>1000 dpf**
WT	0	0	27.3%	60.9%
aqp0a$^{-/-}$	0	42.9%	50.0%	–
aqp0b$^{-/-}$	0	0	22.2%	90.0%
aqp0a$^{-/-}$/ *aqp0b*$^{-/-}$	14.3%	92.9%	89.5%	–

Table 3. *P* Values Calculated Using Fisher's Exact Test for Estimating the Statistical Significance of the Incidence Rate of Dysfunctional GRIN Profiles Between Pairs of Genotypes in Different Age Groups

	Age Group			
Genotype Comparison	**0–200 dpf**	**200–500 dpf**	**500–900 dpf**	**>1000 dpf**
WT versus *aqp0a*$^{-/-}$	$P = 1$	$P = 0.0015^{*}$	$P = 0.2655$	—
WT versus *aqp0b*$^{-/-}$	$P = 1$	$P = 1$	$P = 1$	$P = 0.7966$
WT versus *aqp0a*$^{-/-}$/ *aqp0b*$^{-/-}$	$P = 0.0278^{*}$	$P << 0.001^{*}$	$P << 0.001^{*}$	—
aqp0a$^{-/-}$ versus *aqp0b*$^{-/-}$	$P = 1$	$P = 0.0171^{*}$	$P = 0.1391$	—
aqp0a$^{-/-}$ versus *aqp0a*$^{-/-}$/ *aqp0b*$^{-/-}$	$P = 0.2383$	$P = 0.0128^{*}$	$P = 0.0316^{*}$	—
aqp0b$^{-/-}$ versus *aqp0a*$^{-/-}$/ *aqp0b*$^{-/-}$	$P = 0.0265^{*}$	$P << 0.001^{*}$	$P << 0.001^{*}$	—

* Statistical significance was considered to be $P < 0.05$.

aqp0a$^{-/-}$/*aqp0b*$^{-/-}$ mutant lenses, as displayed in the two orthogonal cross-sectional planes of four selected lenses with diameters of 220 µm (15 dpf), 520 µm (139 dpf), 550 µm (713 dpf), and 660 µm (505 dpf) (Fig. 4). The youngest lens (15 dpf) was larger at 220 µm (Figs. 4A, B; Supplementary Figs. S2E, F) than the two youngest single mutant lenses at 19 dpf (Figs. 2A, B; Figs. 3A, B). This was also supported by the steeper lens growth curve in younger fish (Fig. 1B). At later developmental stages, the rate of lens growth in double *aqp0a*$^{-/-}$/*aqp0b*$^{-/-}$ mutants decreased such that lens growth lagged behind lenses of other genotypes. Refractive index distributions showed various defects, including an asymmetric GRIN profile in the 520-µm lens (Figs. 4C, D), an apparent indentation in the mesh plot that separated the GRIN profile of the 550-µm lens into two distinct regions (Figs. 4E, F), and a dip in the center of the mesh plot of the 660-µm lens. The innermost contour of the two older lenses showed a slight decentration in the 90° orientations (Figs. 4F, H). Two-dimensional contour plots and 3D GRIN profiles were obtained from WT lenses covering an age range similar to that of the MZ mutant lenses (Supplementary Fig. S3).

Statistical analyses of differences in the GRIN profile between lenses from WT and MZ mutant zebrafish lenses were conducted by calculating the incidence rate of disrupted or distorted GRIN profiles that would lead to optical dysfunction and comparing this across the cohorts. (Examples of dysfunctional GRIN profiles are shown in Supplementary Fig. S4.) Samples from each genotype were divided into four age groups: 0 to 200 dpf, 200 to 500 dpf, 500 to 900 dpf, and above 1000 dpf. Also, frequencies of dysfunctional GRIN profiles were compared between the WT and mutant cohorts (Table 2). Disturbances to the GRIN were seen in older WT lenses and found in over 60% of the very old zebrafish (Table 2). A similar trend was seen for lenses from *aqp0b*$^{-/-}$ mutants, but the incidence of a dysfunctional GRIN profile was higher in this mutant cohort than in WT for lenses from animals >1000 dpf. GRIN profiles in lenses from *aqp0a*$^{-/-}$ mutants show disruptions at younger ages, with over 40% of lenses at 200 to 500 dpf and 50% of the lenses with a dysfunctional GRIN at 500 to 900 dpf. Double mutants exhibit disturbed GRIN profiles from very young ages, and this rises to around 90% in the older cohorts.

Fisher's exact test was performed among the six combinations of genotypes in each age group (Table 3). Statistically significant differences were found at all ages between the WT and double mutant GRIN profiles and between *aqp0b*$^{-/-}$ and double mutants. In contrast, statistically significant differences in the GRIN profile were found only at 200 to 500 dpf between WT and *aqp0a*$^{-/-}$ mutants and between *aqp0a*$^{-/-}$ and *aqp0b*$^{-/-}$ mutants. There were no statistically significant differences in the GRIN profiles between WT and *aqp0b*$^{-/-}$ mutants (Table 3).

The maximum refractive index, plotted against both the age and lens diameter for all three mutants, was compared with the values of WT lenses (Figs. 5A, B; fitting coefficients are listed in Table 4). The maximum refractive index increased rapidly in *aqp0a*$^{-/-}$ and *aqp0b*$^{-/-}$ mutant lenses in larval fish and eventually plateaued when lens size exceeded 500 to 600 µm (Fig. 5A) and at ages beyond 120 dpf (Fig. 5B). More variations of maximum refractive index were seen in older *aqp0a*$^{-/-}$ lenses of sizes larger than 800 µm (Fig. 5A). Maximum refractive index growth was delayed and reduced in double *aqp0a*$^{-/-}$/*aqp0b*$^{-/-}$ mutants compared to all other genotypes. Growth of maximum refractive index in the *aqp0b*$^{-/-}$ lens was closest to that of the WT lens.

Cataracts and Defects in the GRIN Profile

The three types of Aqp0 mutants and extremely old WT zebrafish showed different types of lens opacities. These were examined in lenses immediately after dissection from living fish with BF and DF optics and used to generate 2D contours and 3D mesh plots (Figs. 6–10). Spoke opacities were observed in extremely old WT lenses (1939 dpf). Indentations can be seen in both the contours and mesh plots, suggesting lower refractive index values in these spoke regions than in the surrounding lens (Fig. 6). These

Investigative Ophthalmology & Visual Science

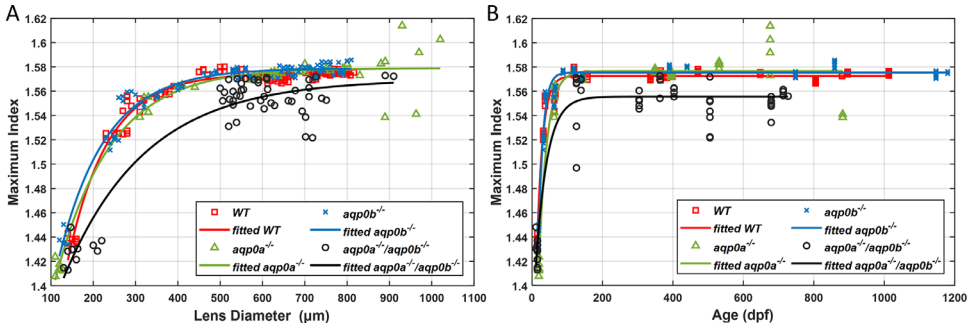

Figure 5. Loss of Aqp0a and Aqp0b alters lens maximum refractive index growth. Lens refractive index as a function of lens diameter (**A**) and age (dpf) (**B**) for WT, *aqp0a*$^{-/-}$, *aqp0b*$^{-/-}$, and double *aqp0a*$^{-/-}$/*aqp0b*$^{-/-}$ mutants. Lens maximum refractive index growth followed a similar trend and plateaued close to 1.58 at lens diameters over ~650 µm (**A**) and in fish over ~40 dpf (**B**). Double *aqp0a*$^{-/-}$/*aqp0b*$^{-/-}$ mutant lens maximum refractive index growth did not plateau and reached a maximum attained value of ~1.57 at lens diameters of ~900 µm (**A**) and fish over ~150 dpf (**B**).

Table 4. Coefficients of Growth in Maximum Refractive Index Fitted to Exponential Growth Model ($y = a + be^{cx}$, r^2) for WT, *aqp0a*$^{-/-}$, *aqp0b*$^{-/-}$, and Double *aqp0a*$^{-/-}$/*aqp0b*$^{-/-}$ Mutants

	Figure 5A, Maximum Refractive Index Versus Lens Diameter				Figure 5B, Maximum Refractive Index Versus Age			
	WT	***aqp0a*$^{-/-}$**	***aqp0b*$^{-/-}$**	***aqp0a*$^{-/-}$/*aqp0b*$^{-/-}$**	**WT**	***aqp0a*$^{-/-}$**	***aqp0b*$^{-/-}$**	***aqp0a*$^{-/-}$/*aqp0b*$^{-/-}$**
a	1.575	1.579	1.579	1.570	1.573	1.577	1.575	1.556
b	–0.672	–0.408	–0.454	–0.321	–0.340	–0.373	–0.584	–0.197
c	–0.011	–0.008	–0.009	–0.005	–0.062	–0.044	–0.077	–0.031
r^2	0.97	0.96	0.97	0.91	0.97	0.96	0.96	0.91

extremely old lenses had diameters of 860 µm and 870 µm, which were larger than found for previously studied WT lenses (750 µm), the oldest of which was 880 dpf.[3]

A pair of *aqp0a*$^{-/-}$ lenses (882 dpf) exhibited both nuclear decentration and anterior polar opacification that corresponded to the localized concentration of refractive index contours and the secondary peak in the mesh plot (Fig. 7). Such disordered distributions of refractive index caused light scattering in the living eye and appeared as severe opacifications (Figs. 7A–C, F–H). Diameters of this *aqp0a*$^{-/-}$ lens pair (960 µm and 890 µm) were much larger than those of comparably aged WT lenses.[3] Spoke cataract was seen in an *aqp0b*$^{-/-}$ lens pair at 1147 dpf (Fig. 8). Similar to the WT lens pair (Fig. 6), indentations that correspond to local lower refractive index regions were found in the contour and mesh plots (Figs. 8D, E, I, J).

Embryonic nuclear opacities were seen in double *aqp0a*$^{-/-}$/*aqp0b*$^{-/-}$ mutant lenses, as shown in an example at 505 dpf (Fig. 9). The corresponding contours and mesh plots exhibited a dip at the center of each lens, indicating a localized lowering of protein concentration in the nucleus. Another pair of double *aqp0a*$^{-/-}$/*aqp0b*$^{-/-}$ mutant lenses (713 dpf) that showed severe opacity across the lenses had asymmetric refractive index contours and

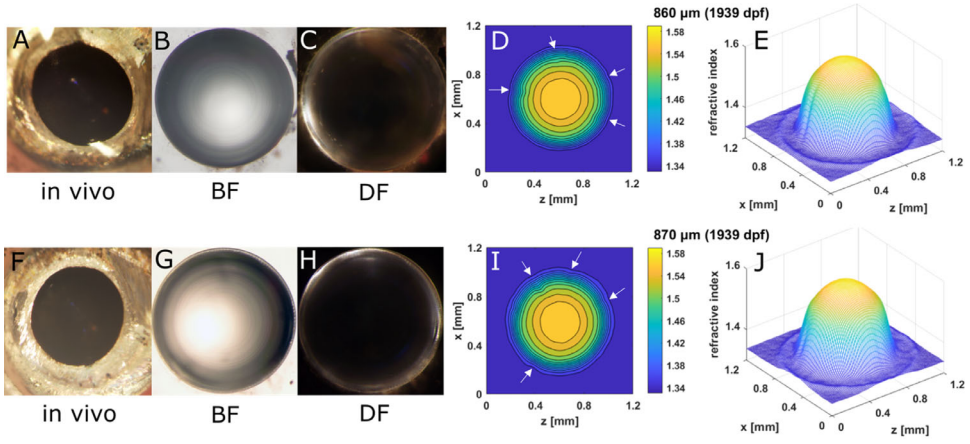

Figure 6. Spoke line opacity in senile WT lenses. (**A**, **F**) In vivo images of eyes of a 27-mm standard length, 1939-dpf old fish, with the corresponding dissected lens pairs illuminated by BF (**B**, **G**) and DF (**C**, **H**) illumination and the corresponding 2D contour plot (**D**, **I**) and 3D mesh plots (**E**, **J**). Spoke opacities are not visible in images taken in vivo because the iris obscures them.

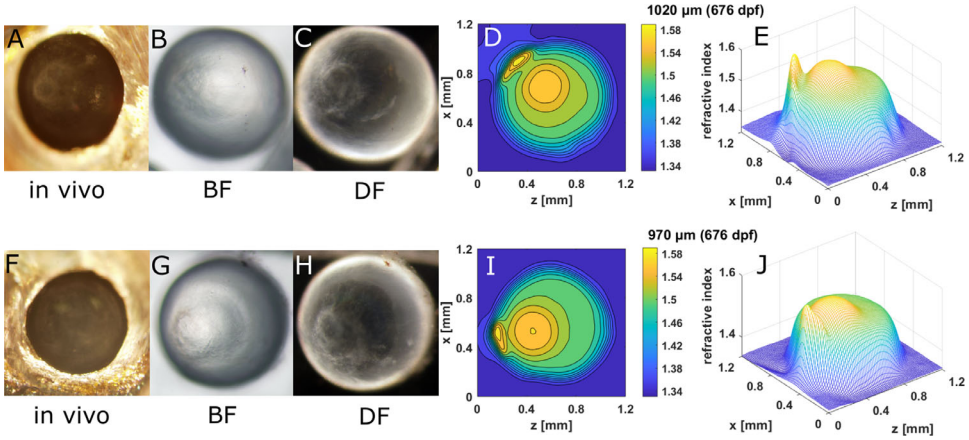

Figure 7. Nuclear asymmetry and anterior polar opacity in old *aqp0a*$^{-/-}$ lenses. (**A**, **F**) In vivo image of eyes of a 28-mm standard length, 676-dpf old *aqp0a*$^{-/-}$ fish, with the corresponding dissected lens pairs imaged by BF (**B**, **G**) and DF (**C**, **H**) illumination and the corresponding 2D contour plot (**D**, **I**) and 3D mesh plots (**E**, **J**) in an axial orientation.

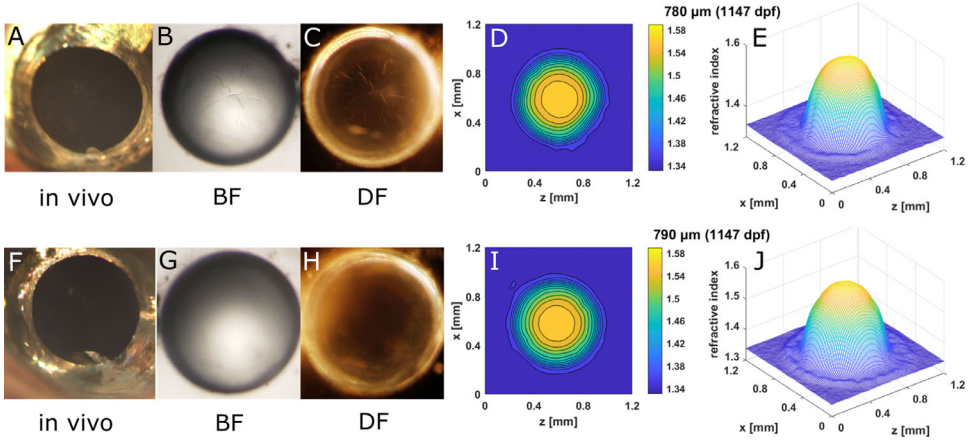

Figure 8. Spoke cataract in old *aqp0b*$^{-/-}$ lenses. (**A**, **F**) In vivo image of eyes of a 21.5-mm standard length, 1147-day old *aqp0b*$^{-/-}$ lens and the corresponding dissected lens pairs imaged by BF (**B**, **G**) and DF (**C**, **H**) illumination and the corresponding 2D contour plot (**D**, **I**) and 3D mesh plots (**E**, **J**). Spoke opacities are not visible in images taken in vivo because the iris obscures them.

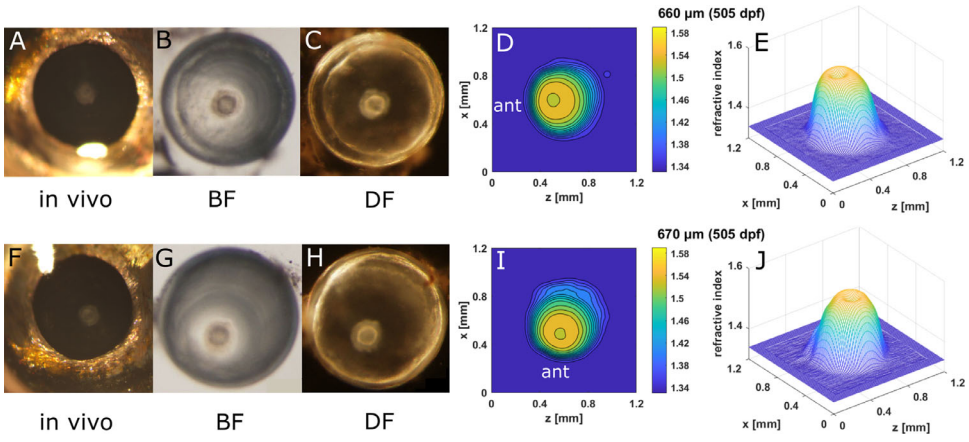

Figure 9. Embryonic nuclear opacity in *aqp0a*$^{-/-}$/*aqp0b*$^{-/-}$ lenses reduced the maximum refractive index in the nucleus. (**A**, **F**) In vivo images of eyes of a 20-mm standard length, 505-dpf old *aqp0a*$^{-/-}$/*aqp0b*$^{-/-}$ fish, with the corresponding dissected lens pairs imaged by BF (**B**, **G**) and DF (**C**, **H**) microscopy and the corresponding 2D contour plots (**D**, **I**) and 3D mesh plots (**E**, **J**).

Investigative Ophthalmology & Visual Science

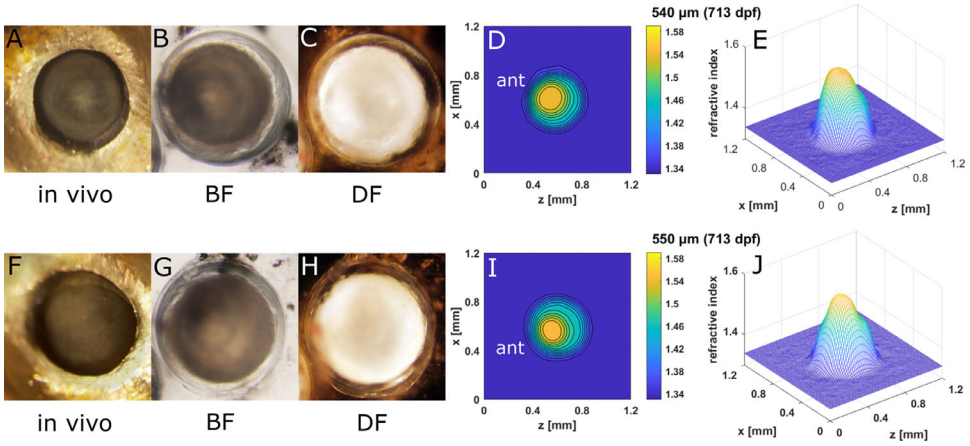

Figure 10. Severe opacity in *aqp0a*$^{-/-}$/*aqp0b*$^{-/-}$ lenses reduced the overall magnitudes of GRIN profiles. (**A**, **F**) In vivo images of eyes of a 21.5-mm standard length, 713-dpf old *aqp0a*$^{-/-}$/*aqp0b*$^{-/-}$ fish, with the corresponding dissected lens pair imaged by BF (**B**, **G**) and DF (**C**, **H**) microscopy and the corresponding 2D contour plots (**D**, **I**) and 3D mesh plots (**E**, **J**).

mesh plots (Fig. 10). The lens sizes and the magnitudes of the GRIN profiles for these severely opaque double *aqp0a*$^{-/-}$/*aqp0b*$^{-/-}$ mutant lens pairs (Figs. 10E, J) were reduced compared to double mutant lenses at a younger age (Figs. 9E, I). Moreover, the shape of the GRIN profile was markedly altered (Supplementary Fig. S5).

Discussion

The shape and material properties of the eye lens determine the refractive power of the eye and the quality of the image that forms on the retina. The gradient distribution of refractive index provides high image quality by significantly reducing aberrations.[34–36] Despite its importance for eye optics and vision, the mechanisms that create and maintain the GRIN profile remain unclear. During development, the lens surface adds new cells in layers with no loss of older existing cells. This layered arrangement, in which cellular protein concentration increases from the periphery to the center of the lens, forms the structural basis for the GRIN. Compaction of inner layers by overlying cells has long been thought to lead to this GRIN profile and in some species may be a contributing factor.[37–39] However, this is not universal, as lenses of nine piscine species, including zebrafish, show no evidence of compaction.[40,41] Alternatively, increased protein synthesis in viable inner lens fiber cells may be a factor and is plausible when growth is rapid and nuclei of inner layer fiber cells have not yet become pyknotic. Zebrafish Aqp0a, but not Aqp0b, requires water transport function to maintain embryonic lens transparency,[24] which in turn impacts the concentration gradients of crystallin proteins. Aqp0b likely facilitates cell-to-cell adhesion in the lens, but loss of function can be compensated by other mechanisms in null mutants, resulting in no morphological phenotype.[26] The sub-functionalization of Aqp0a and Aqp0b in zebrafish provides a unique opportunity to investigate spatially distinct functions of Aqp0 and their regional regulation of the GRIN profile.

Our previous study revealed smooth and symmetric GRIN profiles in WT zebrafish lenses continuously from 15 to 880 dpf.[3] Such an uninterrupted variation in refractive index is essential for maintaining unimpeded refraction in the eye; any irregularities in the GRIN can result in light scatter, which appears as an opacification or cataract that deteriorates image quality. Using functional knockouts of *aqp0a* and/or *aqp0b* from larval to elderly adult stages, this study revealed asymmetric and unsmooth GRIN profiles in different genotypes that manifested as various types of opacities. Extremely old WT lenses and single *aqp0b*$^{-/-}$ mutant lenses tended to show spoke-like opacifications. Single *aqp0a*$^{-/-}$ mutant lenses developed anterior polar opacities and preserved nuclear asymmetry along the anterior–posterior axis at older ages. Double *aqp0a*$^{-/-}$/*aqp0b*$^{-/-}$ mutant lenses exhibited embryonic nuclear opacity, nuclear asymmetry, and severe opacification in adulthood. Lens size and development of GRIN profiles in single *aqp0b*$^{-/-}$ mutants were similar to those of WT zebrafish. Conversely, lenses were smaller in the single *aqp0a*$^{-/-}$ mutants than in the WT and single *aqp0b*$^{-/-}$ mutants. Lens size and maximum refractive index continued to increase beyond ages at which they plateaued in WT, and there was more variation in the GRIN profile in older lenses. Double *aqp0a*$^{-/-}$/*aqp0b*$^{-/-}$ mutants had larger lenses with lower refractive indices across the GRIN profile at younger stages of development compared to WT lenses, but by adulthood both size and refractive index were lower in double *aqp0a*$^{-/-}$/*aqp0b*$^{-/-}$ mutants than in WT or lenses of other genotypes.

Aqp0a Regulated the Symmetric GRIN Profile

The lens is avascular and relies on internal fluid circulation to deliver nutrients and remove waste products.[43,44] All species measured so far have a gradient of hydrostatic pressure.[45] This pressure gradient is modulated by transient receptor potential vanilloid 1 (TRPV1) and TRPV4 channels and the activity of sodium, potassium adenosine triphosphatase (Na,K-ATPase),[46] sodium–potassium–chloride cotransporter 1 (NKCC1), and connexin.[47] Although the role of AQP0 in maintaining the pressure gradient remains unclear, the present work shows that AQP0 clearly plays an essential role in determining the GRIN and thus likely responds to or modulates the pressure gradient.

Aqp0a is required for centralization of the lens nucleus, which forms closer to the anterior pole and progressively shifts to the center with development.[26] This would explain why *aqp0a*$^{-/-}$ mutants have asymmetric GRIN profiles in

the central peak index regions that lie closer to the anterior pole (Fig. 2). Absence of Aqp0a does not alter the magnitude of the GRIN profile (Fig. 5). However, older *aqp0a*$^{-/-}$ lenses tend to develop a secondary high peak index region close to the anterior pole (Fig. 2H), and their corresponding in vivo images reveal anterior polar opacities (Fig. 7). Nuclear centralization is likely essential for maintaining an emmetropic eye during synchronized development in the size of the lens and the eyeball.[26] Appearance of the secondary peak index region could be a consequence of the failure of *aqp0a*$^{-/-}$ mutant lenses to centralize the nucleus.

Our results confirm that Aqp0a plays a critical role in the GRIN profile by centralizing the lens nucleus via proper alignment of lens fiber cells surrounding the lens cortex and by stabilizing the anterior suture. Previous results suggest that water channel functions are mainly regulated by Aqp0a but not Aqp0b in the zebrafish lens.[24,25] It is therefore conceivable that Aqp0a transports water into the differentiating fiber cells, elongating them toward the anterior pole and forcing the nucleus to move posteriorly. Loss of this function causes the lens nucleus to be fixed at the anterior pole, and with age this leads to instability and breakdown of the anterior suture, accumulation of lens nuclear mass,[26] and anterior cataract. Disruption of lens morphology and likely distribution and concentration of crystallins at the anterior pole result in the secondary, age-related GRIN peak that we observed. Interestingly, zebrafish lenses over ~900 dpf burst, leaving behind a clump of lens nuclear tissue and a lens capsule with a disintegrating cortex. Hence, we were unable to measure GRIN in very old *aqp0a*$^{-/-}$ mutants. It is likely that the increasingly unstable anterior suture allowed the lens to swell due to high hydrostatic pressure and then eventually burst beyond a critical age/size. Our findings suggest that the water channel function of Aqp0a is of crucial importance for maintaining optical function in the lens cortex.

Both Aqp0a and Aqp0b Regulate the GRIN Plateau Region

In young larval zebrafish, a sharp and symmetric GRIN profile formed in the absence of either or both Aqp0a and Aqp0b (Supplementary Fig. S2). The lens size of the double mutants was larger than that of the single mutants (Supplementary Fig. S2) and WT lenses.[3] This is likely caused by a loss in cell volume regulation so that either lens cells swell or there is more water accumulation in the extracellular space.[26] Water content and extracellular space also increased in *AQP0*$^{+/-}$ and *AQP0*$^{+/-}$*/AQP1*$^{+/-}$mutations in murine lenses.[17] Later, in juveniles, the magnitude of the central plateau region in GRIN profiles of double *aqp0a*$^{-/-}$*/aqp0b*$^{-/-}$ mutants was consistently reduced when compared with other genotypes (Fig. 5) and sometimes dipped in the center (Figs. 4H, 9). This suggests that at least one of the two Aqp0s is required for the lens to generate a high crystallin concentration to attain the peak refractive index value of around 1.58. Aqp0s are membrane proteins and are not involved with the synthesis of crystallin proteins in the cytosol. However, alterations in water transport would result in changes in the water-to-protein ratio in the lens nucleus and could lead to macromolecular crowding required to generate the correct optics in the plateau region. It is also plausible that defects in a shared role in structural integrity, such as cell-to-cell adhesion, would lead to inadequate packing of the lens nucleus and a lower maximum GRIN.

In mammalian lenses, Aqp0 undergoes C-termini truncations that facilitate the formation of abundant thin junctions in the lens center that are likely to convert the Aqp0 proteins into pure adhesion molecules.[6] C-termini signal loss of both Aqp0a and Aqp0b proteins has been reported in mature fiber cells of zebrafish.[26] Loss of a single Aqp0 protein does not reduce the magnitude of refractive index in the lens center, suggesting that both Aqp0s have a similar function and hence can compensate one another in the central regions of the lens. Cellular fusions are found in deeper lens regions,[48,49] suggesting that there may be some cytosolic constituents shared between central fiber cells. If this is also the case in zebrafish lens, both Aqp0a and Aqp0b are likely to play a major role in maintaining optical function in the lens center.

Although this study investigated how mutations in Aqp0s affect the GRIN, these membrane proteins do not exert their effects in isolation and are likely to impact or be influenced by other lens proteins, including cytoplasmic and intermediate filament proteins. AQP0 regulates the function of connexin,[50,51] which is crucial for lens development, transparency, and cell-to-cell adhesion.[52] AQP0 also anchors the intermediate protein filensin.[53,54] AQP0 may also directly or indirectly affect other lens proteins, such as the lens intrinsic membrane protein 2 (LIM2), also known as MP20, which has been found to play a role in both cell fusion and the organizational structure of the lens into syncytia.[55] These cellular groupings are stratified and aid in intracellular diffusion within each stratum. In the murine lens, LIM2 creates a tripartite syncytial arrangement of surface layer proteins.[55] Such a tripartite arrangement and the role of LIM2 in its formation have been implicated in the formation of the GRIN by ensuring a uniform refractive index within each stratum, corresponding to concentric isoindicial contours seen in WT lenses.[3] The plateau region that we observe in the lens center that develops with age can be explained, at least in part, by the central syncytium that allows relatively unrestricted movement of proteins.[55] This has also been observed in developing chicken lenses in which cytoplasmic and membrane proteins diffused freely[56] and appears to correspond to the development of a central plateau of uniform refractive index in the GRIN of the developing lens.[39] Diffusion of large molecules may be facilitated by cell–cell fusions in lenses of many species.[48,49,57] Such fusions may be fundamental in the formation of lens column bifurcation points and integral to development of the lenticular architecture[49] critical for formation of the GRIN.[56]

We propose that in the lens cortex of the zebrafish Aqp0a plays the major water transport role, regulating centralization of the GRIN plateau region and symmetry of the GRIN profile. Our findings also suggest that, in the lens center, Aqp0a and Aqp0b have a common function as adhesive molecules in the primary lens fiber cells to maintain the development of the GRIN central plateau region. In addition, lens growth is likely to be stepwise rather than continuous, as evidenced by the larger lens diameters in the extremely old lenses, which may provide mutant lenses the opportunity to compensate for malfunctioning mechanisms in periods when growth is slower or dormant. Interactions with other proteins, such as connexins, intermediate filament proteins, and LIM2, regionally restricted within the lens, may contribute to these spatially restricted functions. Future studies examining interactions between Aqp0s and

Investigative Ophthalmology & Visual Science

these potential functional partners will help reveal region-restricted functions of Aqp0s in development of the lens refractive index.

Acknowledgments

The authors thank Ines Gehring for the zebrafish husbandry.

Supported by beam time grants at SPring-8 (2016A1096, 2017A1197, 2018A1105, 2019A1115) and by grants from the Royal Society (IE160996), Fight for Sight UK (1319/1320), National Natural Science Foundation of China (82000878), and National Institutes of Health (R01 EY05661).

Disclosure: **K. Wang**, None; **I. Vorontsova**, None; **M. Hoshino**, None; **K. Uesugi**, None; **N. Yagi**, None; **J.E. Hall**, None; **T.F. Schilling**, None; **B.K. Pierscionek**, None

References

1. Bassnett S, Šikić H. The lens growth process. *Prog Retin Eye Res*. 2017;60:181–200.
2. Pierscionek BK, Regini JW. The gradient index lens of the eye: an opto-biological synchrony. *Prog Retin Eye Res*. 2012;31(4):332–349.
3. Wang K, Vorontsova I, Hoshino M, et al. Optical development in the zebrafish eye lens. *FASEB J*. 2020;34(4):5552–5562.
4. Wages P, Horwitz J, Ding L, Corbin RW, Posner M. Changes in zebrafish (*Danio rerio*) lens crystalline content during development. *Mol Vis*. 2013;19:408–417.
5. Michael R, van Marle J, Vrensen GF, van den Berg TJ. Changes in the refractive index of lens fibre membranes during maturation–impact on lens transparency. *Exp Eye Res*. 2003;77(1):93–99.
6. Engel A, Fujiyoshi Y, Gonen T, Walz T. Junction-forming aquaporins. *Curr Opin Struct Biol*. 2008;18(2):229–235.
7. Petrova RS, Schey KL, Donaldson PJ, Grey AC. Spatial distributions of AQP5 and AQP0 in embryonic and postnatal mouse lens development. *Exp Eye Res*. 2015;132:124–135.
8. Bok D, Dockstader J, Horwitz J. Immunocytochemical localization of the lens main intrinsic polypeptide (MIP26) in communicating junctions. *J Cell Biol*. 1982;92(1):213–220.
9. Lo WK, Biswas SK, Brako L, Shiels A, Gu S, Jiang JX. Aquaporin-0 targets interlocking domains to control the integrity and transparency of the eye lens. *Invest Ophthalmol Vis Sci*. 2014;55(3):1202–1212.
10. Kumari SS, Varadaraj K. Intact AQP0 performs cell-to-cell adhesion. *Biochem Biophys Res Comm*. 2009;390(3):1034–1039.
11. Nakazawa Y, Oka M, Funakoshi-Tago M, Tamura H, Takehana M. The extracellular C-loop domain plays an important role in the cell adhesion function of Aquaporin 0. *Curr Eye Res*. 2017;42(4):617–624.
12. Lindsey Rose KM, Gourdie RG, Prescott AR, Quinlan RA, Crouch RK, Schey KL. The C terminus of lens Aquaporin 0 interacts with the cytoskeletal proteins filensin and CP49. *Invest Ophthalmol Vis Sci*. 2006;47(4):1562–1570.
13. Nakazawa Y, Oka M, Furuki K, Mitsuishi A, Nakashima E, Takehana M. The effect of the interaction between Aquaporin 0 (AQP0) and the filensin tail region on AQP0 water permeability. *Mol Vis*. 2011;17:3191–3199.
14. Yu XS, Jiang JX. Interaction of major intrinsic protein (aquaporin-0) with fiber connexins in lens development. *J Cell Sci*. 2004;117:871–880.
15. Liu J, Xu J, Gu S, Nicholson BJ, Jiang JX. Aquaporin 0 enhances gap junction coupling via its cell adhesion function and interaction with connexin 50. *J Cell Sci*. 2011;124:198–206.
16. Kumari SS, Gupta N, Shiels A, et al. Role of Aquaporin 0 in lens biomechanics. *Biochem Biophys Res Comm*. 2015;462(4):339–345.
17. Kumari SS, Varadaraj K. Aquaporin 0 plays a pivotal role in refractive index gradient development in mammalian eye lens to prevent spherical aberration. *Biochem Biophys Res Comm*. 2014;452(4):986–991.
18. Shiels A, Bassnett S, Varadaraj K, et al. Optical dysfunction of the crystalline lens in aquaporin-0-deficient mice. *Physiol Genomics*. 2001;7(2):179–186.
19. Grey AC, Li L, Jacobs MD, Schey KL, Donaldson PJ. Differentiation-dependent modification and subcellular distribution of aquaporin-0 suggests multiple functional roles in the rat lens. *Differentiation*. 2009;77(1):70–83.
20. Ball LE, Little M, Nowak MW, Garland DL, Crouch RK, Schey KL. Water permeability of C-terminally truncated aquaporin 0 (AQP0 1-243) observed in the aging human lens. *Invest Ophthalmol Vis Sci*. 2003;44(11):4820–4828.
21. Schey K, Petrova R, Gletten R, Donaldson P. The role of aquaporins in ocular lens homeostasis. *Int J Mol Sci*. 2017;18(12):2693.
22. Amores A, Force A, Yan YL, et al. Zebrafish hox clusters and vertebrate genome evolution. *Science*. 1998;282(5394):1711–1714.
23. Vihtelic TS, Fadool JM, Gao J, Thornton KA, Hyde DR, Wistow G. Expressed sequence tag analysis of zebrafish eye tissues for NEIBank. *Mol Vis*. 2005;11:1083–1100
24. Clemens DM, Németh-Cahalan KL, Trinh L, Zhang T, Schilling TF, Hall JE. In vivo analysis of aquaporin 0 function in zebrafish: permeability regulation is required for lens transparency. *Invest Ophthalmol Vis Sci*. 2013;54(7):5136–5143.
25. Froger A, Clemens D, Kalman K, Németh-Cahalan KL, Schilling TF, Hall JE. Two distinct aquaporin 0s required for development and transparency of the zebrafish lens. *Invest Ophthalmol Vis Sci*. 2010;51(12):6582–6592.
26. Vorontsova I, Gehring I, Hall JE, Schilling TE. Aqp0a regulates suture stability in the zebrafish lens. *Invest Ophthalmol Vis Sci*. 2018;59(7):2869–2879.
27. Westerfield M. *The Zebrafish Book: A Guide for the Laboratory Use of Zebrafish (Danio rerio)*. Eugene, OR: University of Oregon Press; 2000.
28. Schilling TF. The morphology of larval and adult zebrafish. In: Nusslein-Volhard C, Dahm R. , eds. *Zebrafish: A Practical Approach*. Oxford: Oxford University Press; 2002:59–94.
29. Momose A, Kawamoto S, Koyama I, Hamaishi Y, Takai K, Suzuki Y. Demonstration of x-ray Talbot interferometry. *Jpn J Appl Phys*. 2003;42:L866–L868.
30. Momose A. Recent advances in x-ray phase imaging. *Jpn J Appl Phys*. 2005;44:6355–6367.
31. Barer R, Joseph S. Refractometry of living cells. Part 1. Basic principles. *Q J Microsc Sci*. 1954;95:399–423.
32. Hoshino M, Uesugi K, Yagi N, Mohri S, Regini J, Pierscionek B. Optical properties of in situ eye lenses measured with x-ray Talbot interferometry: a novel measure of growth processes. *PLoS One*. 2011;6(9):e25140.
33. Hoshino M, Uesugi K, Yagi N, Mohri S. Investigation of imaging properties of mouse eyes using X-ray phase contrast tomography. In: *AIP Conference Proceedings*. New York: American Institute of Physics; 2010:57–61.
34. Birkenfeld J, De Castro A, Ortiz S, Pascual D, Marcos S. Contribution of the gradient refractive index and shape to the crystalline lens spherical aberration and astigmatism. *Vision Res*. 2013;86:27–34.
35. Birkenfeld J, de Castro A, Marcos S. Contribution of shape and gradient refractive index to the spherical aberration

Investigative Ophthalmology & Visual Science

of isolated human lenses. *Invest Ophthalmol Vis Sci*. 2014;55(4):2599–2607.

36. Fernald RD, Wright SE. Maintenance of optical quality during crystalline lens growth. *Nature*. 1983;301(5901):618–620.
37. Al-Ghoul KJ, Nordgren RK, Kuszak AJ, Freel CD, Costello MJ, Kuszak JR. Structural evidence of human nuclear fiber compaction as a function of ageing and cataractogenesis. *Exp Eye Res*. 2001;72(3):199–214.
38. Costello MJ, Mohamed A, Gilliland KO, Fowler WC, Johnsen S. Ultrastructural analysis of the human lens fiber cell remodelling zone and the initiation of cellular compaction. *Exp Eye Res*. 2013;116, 411–418.
39. Wang K, Hoshino M, Uesugi K, et al. Cell compaction is not required for the development of gradient refractive index profiles in the embryonic chick lens. *Exp Eye Res*. 2020;197:108–112.
40. Kozłowski TM, Kröger RH. Constant lens fiber cell thickness in fish suggests crystallin transport to denucleated cells. *Vis Res*. 2019;162:29–34.
41. Kozłowski TM, Kröger RH. Visualization of adult fish lens fiber cells. *Exp Eye Res*. 2019;181:1–4.
42. Nemeth-Cahalan KL, Clemens DM, Hall JE. Regulation of AQP0 water permeability is enhanced by cooperativity. *J Gen Physiol*. 2013;141(3):287–295.
43. Donaldson P, Kistler J, Mathias RT. Molecular solutions to mammalian lens transparency. *News Physiol Sci*. 2001;16:118–123.
44. Mathias RT, Kistler J, Donaldson P. The lens circulation. *J Membr Biol*. 2007;216(1):1–16.
45. Gao J, Sun X, Moore LC, Brink PR, White TW, Mathias RT. The effect of size and species on lens intracellular hydrostatic pressure. *Invest Ophthalmol Vis Sci*. 2013;54(1):183–192.
46. Gao J, Sun X, White TW, Delamere NA, Mathias RT. Feedback regulation of intracellular hydrostatic pressure in surface cells of the lens. *Biophys J*. 2015;109(9):1830–1839.
47. Delamere NA, Shahidullah M, Mathias RT, et al. Signaling between TRPV1/TRPV4 and intracellular hydrostatic pressure in the mouse lens. *Invest Ophthalmol Vis Sci*. 2020;61(6):58.
48. Kuszak JR, Macsai MS, Bloom K, Rae J, Weinstein R. Cell-to-cell fusion of lens fiber cells in situ: correlative light, scanning electron microscopic, and freeze fracture studies. *J Ultrastruct Res*. 1985;93(3):144–160.
49. Kuszak JR, Ennesser CA, Bertram BA, Imherr-McMannis S, Jones-Rufer LS, Weinstein RS. The contribution of cell-to-cell fusion to the ordered structure of the crystalline lens. *Lens Eye Toxic Res*. 1989;6(4):639–673.
50. Yu XS, Jiang JX. Interaction of major intrinsic protein (aquaporin-0) with fiber connexins in lens development. *J Cell Sci*. 2004;117:871–880.
51. Liu J, Xu J, Gu S, Nicholson BJ, Jiang JX. Aquaporin 0 enhances gap junction coupling via its cell adhesion function and interaction with connexin 50. *J Cell Sci*. 2011;124:198–206.
52. Hu Z, Shi W, Riquelme MA, et al. Connexin 50 functions as an adhesive molecule and promotes lens cell differentiation. *Sci Rep*. 2017;7(1):5298.
53. Lindsey Rose KM, Gourdie RG, Prescott AR, Quinlan RA, Crouch RK, Schey KL. The C terminus of lens aquaporin 0 interacts with the cytoskeletal proteins filensin and CP49. *Invest Ophthalmol Vis Sci*. 2006;47(4):1562–1570.
54. Nakazawa Y, Oka M, Furuki K, Mitsuishi A, Nakashima E, Takehana M. The effect of the interaction between Aquaporin 0 (AQP0) and the filensin tail region on AQP0 water permeability. *Mol Vis*. 2011;17:3191–3199.
55. Shi Y, Barton K, De Maria A, Petrash JM, Shiels A, Bassnett S. The stratified syncytium of the vertebrate lens. *J Cell Sci*. 2009;122:1607–1615.
56. Shestopalov VI, Bassnett S. Expression of autofluorescent proteins reveals a novel protein permeable pathway between cells in the lens core. *J Cell Sci*. 2000;113:1913–1921.
57. Kuszak JR. The ultrastructure of epithelial and fiber cells in the crystalline lens. *Int Rev Cytol*. 1995;163:305–350.

Investigative Ophthalmology & Visual Science